Neon radiation efficiency for different confinement regimes in TEXTOR-94

G. Telesca[a*], B. Unterberg[b], R. Jaspers[c], A.M. Messiaen[a], J. Ongena[a], J. Rapp[b], U. Samm[b], N. Schoon[a], M. Lehnen[b], M. Tokar'[b], G. Van Oost[a], R. Zagorski[d]

[a] Laboratoire de physique des Plasmas/Laboratorium voor Plasmafysica, Ecole Royale Militaire/Koninklijke Militaire School, Euratom Association, Brussels, Belgium**

[b] Institut für Plasmaphysik, Forschungszentrum Jülich GmbH, Euratom Association, Jülich, Germany**

[c] FOM-Instituut voor Plasmafysica, Rijnhuizen, Euratom Association, Nieuwegein, Netherlands**

[d] Institute of Plasma Physics and Laser Microfusion, Warsaw, Poland

Abstract. For neon seeded discharges the quantity $[\Delta P_{rad}/\Delta Z_{eff}(0)]/\bar{n}_{e0}^2$, which depends linearly on the effective neon cooling rates and which can be taken as a measure of the radiation efficiency of neon, is not a constant for a given machine. When, according to the mode of operation, $[\Delta P_{rad}/\Delta Z_{eff}(0)]/\bar{n}_{e0}^2$ is high, radiative power exhaust can be efficiently achieved at low Z_{eff}. The value of this ratio, which we refer to as the quality of neon cooling, is found to be correlated not only with the plasma edge temperature but also, and even more strongly, with the confinement properties of the discharges. Two different high confinement radiative regimes in TEXTOR-94 have been compared: radiative improved (RI) mode (highest confinement) and gas puff/pure radiofrequency mode (slightly lower confinement). Although the electron temperature profile is similar in the two regimes, due to feedback control of the input power level, it has been found experimentally that the quality of neon cooling is lower for the RI mode than for the gas puff/pure radiofrequency one. Similar behaviour has been observed for the quality of cooling of the residual intrinsic carbon, determined with independent diagnostics and methods. Simulations with the self-consistent RITM code confirm that particle transport, in particular the perpendicular diffusivity at the edge, is a key parameter to determine the level of the power radiated at the edge for a given impurity concentration in the plasma core.

1. Introduction

Impurity seeding of a deuterium plasma may represent a solution to the problem of power exhaust in a fusion reactor: when electronic excitation of impurity ions occurs predominantly at the plasma periphery, a relevant fraction of the plasma edge thermal power, which would normally be transferred to the targets, can be converted into radiation. Due to the isotropic character of line emission, this can result in a strong reduction of the peak heat load on the targets since the power is distributed more homogeneously over the walls [1]. If, as in the first experiments of neon injection on TEXTOR [1], energy confinement is practically unaffected by impurity seeding, the critical parameter for the viability of the radiative mantle concept can be identified in the level of the incremental ionic effective charge in the plasma centre, $\Delta Z_{eff}(0)$. More precisely, the value of the ratio between the incremental radiated power at the plasma edge, ΔP_{rad}, and $\Delta Z_{eff}(0)$ was found to be the figure of merit [2].

Experiments on limiter tokamaks such as TEXTOR-94 [3] and TFTR [4], however, as well as on divertor tokamaks such as JET [5] and ASDEX Upgrade [6] have shown that a change of energy confinement may occur when impurities are seeded. This depends on a variety of variables such as the atomic number of the seeded impurity, the level of the total input power and of the power radiated, the location of the plasma volume where most of the radiation is emitted and the level of the electron density. Moreover it may happen, as for example in TEXTOR-94 [7] and in ASDEX Upgrade [8], that changes in the regime of confinement are correlated with changes in the level of the ratio $\Delta P_{rad}/\Delta Z_{eff}(0)$. Therefore, in comparing different radiative scenarios both the difference in confinement and the change in the level

[*] *Present affiliation:* Consorzio RFX, Padova, Italy.

[**] Partners in the Trilateral Euregio Cluster.

of $\Delta P_{rad}/\Delta Z_{eff}(0)$ have to be taken into account in order to evaluate consistently their benefits and disadvantages.

As a general trend, when low–medium-Z impurities are seeded in divertor tokamaks and radiation is mostly localized in the divertor zone and/or in the vicinity of the X point the energy confinement decreases or remains unchanged, while a beneficial effect on confinement can be obtained when a significant fraction of radiated power is emitted inside the LCFS. In this case, H mode performance can be extended up to high density regimes [9, 10]. In limiter tokamaks confinement can substantially increase as in TEXTOR-94, where the radiative improved (RI) mode has been achieved [3], and as in TFTR, where experiments with neon seeding at high density have given indications of enhanced confinement [4].

Although the experimental data show that a certain incompatibility may arise between extremely high confinement radiative regimes and a reasonably low level of Z_{eff} [7, 8], in TEXTOR-94 radiative scenarios can be produced in which good confinement is combined with a tolerable level of Z_{eff}.

Since for a given impurity density $P_{rad} \propto n_e$ and $Z_{eff} - 1 \propto n_e^{-1}$ (n_e is the electron density) $\Delta P_{rad}/\Delta Z_{eff}(0)$ scales as n_e^2. Therefore the normalized ratio $[\Delta P_{rad}/\Delta Z_{eff}(0)]/\bar{n}_{e0}^2$ ($\bar{n}_{e0}$ is the central line averaged electron density), which does not depend explicitly on n_e, turns out to be the relevant quantity to be used when discharges of different densities are compared. The normalized ratio, which for an impurity i of charge Z_i is equal to $[L_i(T_e)/(Z_i^2 - Z_i)]V_L$ ($L_i(T_e)$ is the average cooling rate in the volume V_L where line radiation is emitted) [11], represents not only a useful quantity but expresses the intrinsic capability of an impurity to radiate in a given scenario. For this reason $[\Delta P_{rad}/\Delta Z_{eff}(0)]/\bar{n}_{e0}^2$ or more simply $\{P_{rad}/[Z_{eff}(0) - 1]\}/\bar{n}_{e0}^2$ will be referred to as the quality of impurity cooling. Indeed, from a practical point of view the use of $\{P_{rad}/[Z_{eff}(0) - 1]\}/\bar{n}_{e0}^2$ is more convenient since the error in the evaluation of ΔZ_{eff} and of ΔP_{rad} (and therefore in the normalized ratio) can be high, especially when the differences in Z_{eff} and in P_{rad} with and without seeded impurities are small. On the other hand, measurements show, in agreement with simple analytical considerations, that $\Delta P_{rad}/\Delta Z_{eff}(0)$ is comparable with $P_{rad}/[Z_{eff}(0) - 1]$ when both P_{rad} and Z_{eff} are dominated by the seeded impurity, as in our case (Section 3.3). For practical purposes the two ratios can, therefore, be considered as equivalent.

We have compared only for very few cases the (global) quality of neon cooling (q.n.c.), measured using bolometry and bremsstrahlung, with the (partial) quality of carbon cooling, measured using independent diagnostics, for that fraction of the original carbon still present in the discharge after neon seeding. This comparison shows a similar trend for the radiation efficiency of carbon and neon with increasing confinement.

In contrast to previous studies on the impurity radiation efficiency (see, e.g., Ref. [11]) a peculiar and significant aspect of the present work consists in the use of a locally determined Z_{eff}. In fact, since the local bremsstrahlung emissivity depends on the local value of n_e^2, a change in the electron density profile, even at $\bar{n}_{e0}$ and Z_{eff} constant, implies a change in the line integrated bremsstrahlung. For that reason a measure of the average Z_{eff}, which is based on the central line integrated electron density and bremsstrahlung [12], can be affected by important relative errors of under/overestimation when, as in our case, discharges of very different electron density profiles are compared. We have therefore developed a new diagnostic for the evaluation of the local Z_{eff} in the plasma centre.

2. Diagnostics

The geometry of the seven viewing chords of the $Z_{eff}(0)$ diagnostic (visible continuum at $\lambda = 5230$ Å) has been chosen in such a way as to avoid detection of local edge radiation emitted from the ALT-II and bumper toroidal limiters, Fig. 1(a). Therefore it is possible to invert the signals using the Abel method, since they are not affected by localized poloidal asymmetries. On the other hand the absence of chords at the very edge of the plasma (the last chord is located 10 cm from the LCFS on the low field side) could in principle cause a significant error in the reconstructed emissivity profile. However, measurements and simulation [13] show that the lack of knowledge of the exact level of the continuum at the plasma edge can cause an important error in the reconstructed emissivity profile only at large minor radii, while in the central plasma the error is at most of a few per cent. Comparison with other diagnostics shows that the total error on the reconstructed bremsstrahlung emissivity in the central plasma, which arises mainly from the limited number of viewing chords and from the absolute calibration, is of the order of 15% for a time resolution of about 30 ms.

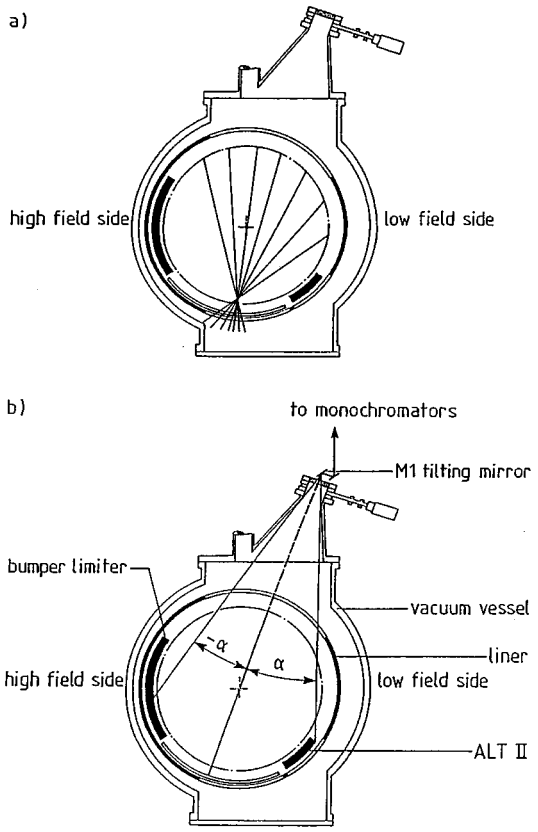

Figure 1. (a) Geometry of the seven viewing chords for the measurement of visible continuum radiation (see text). (b) Experimental set-up for the simultaneous measurement of the brilliance of three carbon lines. The line of sight scans the whole plasma cross-section at a repetition time of 150 ms.

In Fig. 1(b) the experimental set-up for the measurement of spectral lines in the visible and ultraviolet is shown. By tilting the mirror M1 the whole plasma cross-section is nearly vertically scanned from the low to the high field side and vice versa with a repetition time of 150 ms. The light from the mirror is focused into the entrance slits of two monochromators, one of which is equipped with two exit slits. Therefore three spectral lines can be detected simultaneously and, for steady state phases, also the spatial distribution of their brilliances is determined. In the present study we report measurements of three carbon lines emitted by C^{2+}, C^{3+} and C^{4+} ions, respectively, at λ = 2296, 5805 and 2271 Å. While the beryllium- and lithium-like C^{2+} and C^{3+} ions are mostly poloidally localized, as is the radiation they emit, in the vicinity of the carbon sources (toroidal limiters, hence poloidal asymmetry), radiation from C^{4+} ions is nearly homogeneously poloidally distributed [14].

The other specific diagnostics used in this study are: helium and lithium thermal beams for the measure of the edge electron temperature and density [15, 16] and a 26 channel bolometric system for the measure of the radiated power P_{rad}, radially and poloidally resolved [17].

3. Experiments

3.1. Radiative modes in TEXTOR-94

For auxiliary heated discharges with neon seeding in TEXTOR-94, when the radiated power fraction $\gamma = P_{rad}/P_{tot}$ exceeds 0.45–0.50 and $\bar{n}_{e0}$ is higher than about 0.7, the Greenwald density ($n_{Gr} = I_p/\pi a^2 \times 10^{20}$ m^{-3}, I_p in MA and a, minor radius, in metres), the energy confinement increases linearly with $\bar{n}_{e0}/n_{Gr}$ if the following conditions are fulfilled [18]:

(a) The rise in electron density must be only due to limiter desorption and/or to very moderate gas puff or to pellet injection [19], explicitly excluding strong gas puff,
(b) At least 25–30% of the total input power must be supplied by neutral beam co-injection, (NB-co).

In such a case (RI mode) the confinement enhancement factor with respect to the ITER H93-P ELM-free scaling f_{H93} is equal to $\bar{n}_{e0}/n_{Gr}$ [3]. In the other cases, namely at high gas puffing rate and/or when the radiofrequency power accounts for more than 0.7–0.8 of P_{tot}, the energy confinement is higher than that predicted by L mode scaling but generally f_{H93} does not exceed 0.80–0.85 even at $\bar{n}_{e0}/n_{Gr}$ slightly above 1.

f_{H93} is correlated (both for RI mode and for gas puff/pure radiofrequency) with the electron density peaking factor, here defined as $f_p = n_e(0)/\bar{n}_{e0}$: when f_p increases from 1.3 to 1.65, f_{H93} increases from about 0.6 to about 1.0. Once the conditions for the RI mode are established at given $\bar{n}_{e0}$ and γ, a further increase in the level of γ does not generally lead to a further increase in f_{H93} and in f_p. The consequences of the increased γ level are limited to a further reduction of the edge electron temperature $T_e(a)$ and to a small decrease of the edge electron density $n_e(a)$ [18], which, however, is not sufficient to modify appreciably f_p.

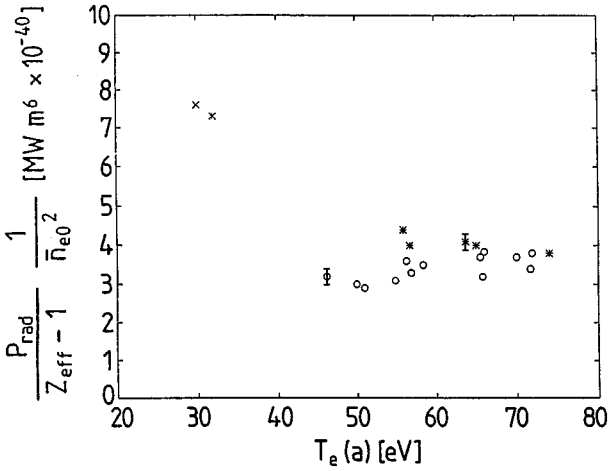

Figure 2. Quality of neon cooling as a function of the edge electron temperature $T_e(a)$ for L mode discharges (crosses) and for gas puff (asterisks) and RI mode (circles) discharges.

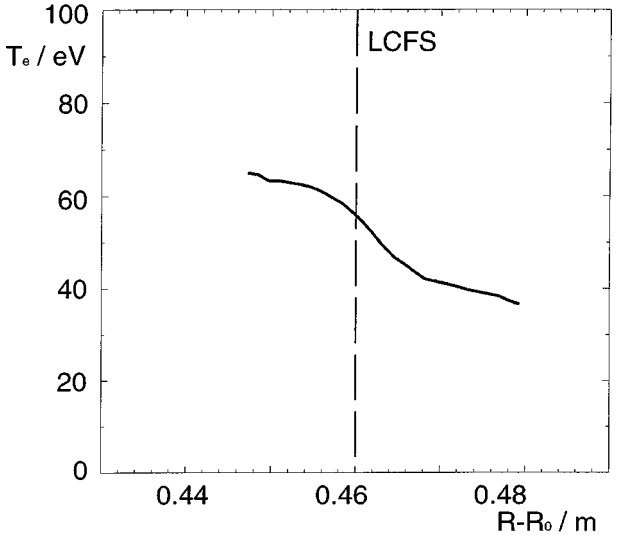

Figure 3. Typical edge electron temperature profile, from a thermal helium beam diagnostic, for high density, high radiated power level discharges in TEXTOR-94. The limiter position is at $r = 46$ cm.

When $\bar{n}_{e0}/n_{Gr}$ is below 0.7 the confinement is lower in all situations and its level is comparable to the L mode scaling.

3.2. The quality of neon cooling

In Fig. 2 the quality of neon cooling (q.n.c. = $\{P_{rad}/[Z_{eff}(0) - 1]\}/\bar{n}_{e0}^2$) for a series of consecutive discharges at $I_p = 400$ kA is shown as a function of electron edge temperature $T_e(a)$. The two data points at $T_e(a)$ about 30 eV refer to L mode discharges with neon seeding at relatively low density ($\bar{n}_{e0} = 4 \times 10^{13}$ cm^{-3}), as compared with the Greenwald density $n_{Gr} = 6 \times 10^{13}$ cm^{-3} at $I_p = 400$ kA and $a = 46$ cm, and at low input power $P_{tot} = 1.3$ MW. The normalized beta for these L mode discharges was low ($\beta_N = 1.1$) as compared with the beta limit for TEXTOR-94 of about 2.0. The other data points in Fig. 2 refer to neon seeded discharges with strong gas puff (asterisks) and to RI mode discharges (circles). All of them, strong gas puff and RI mode, display higher density ($\bar{n}_{e0}$ comparable with n_{Gr}), higher beta ($\beta_N = 1.5$), higher input power (P_{tot} up to 3 MW) and higher confinement ($f_{H93} = 0.8$–1.0). In contrast to other experimental situations, reported in Ref. [11], the two L mode data of Fig. 2 refer to temperatures lower than those of the discharges at higher confinement. Consequently, since the neon cooling rate is a decreasing function of temperature, the L mode data of Fig. 2 cannot provide information about the influence of transport on the level of the q.n.c.

The most relevant feature of all the discharges considered in the present study (with the exception of the two above mentioned L mode ones) consists in the similarity of their electron temperature profile, although the discharges differ in confinement. In fact, on the one hand, a feedback control of the auxiliary power level assures that the stored energy is not in excess of 125 kJ and, on the other hand, the contribution of fast ions to the total plasma energy is negligible for these high density discharges, as indicated by TRANSP calculations [3]. Furthermore, there are no experimental indications that the ratio T_i/T_e changes significantly on comparing discharges with f_{H93} in the range 0.8–1. The strong collisional coupling between electrons and ions at the very high density considered leads to a ratio T_i/T_e close to one independent of energy confinement. The stored energy level of 125 kJ is achieved in the discharges (RI mode and non-RI mode) at the highest densities, $\bar{n}_{e0}$ about 6×10^{19} m^{-3}, while at lower densities the stored energy is proportionally lower. The typical central plasma electron temperature is 1.3–1.5 keV (generally RI mode discharges have a slightly higher core temperature) and the temperature at $r = 34$ cm ($r/a = 0.74$), where the most outward channel of the electron cyclotron emission diagnostic is located, is about 400 eV. At the LCFS the thermal helium beam diagnostic shows remarkable differences in electron temperature, in the range 50–80 eV. $T_e(a)$ depends, indeed, mainly on the level

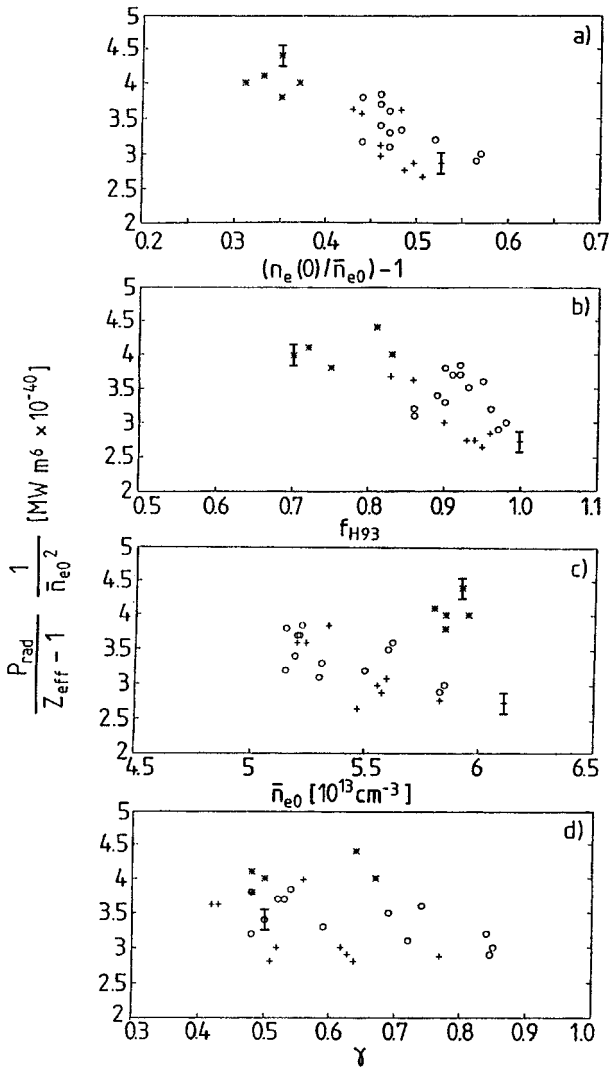

Figure 4. Quality of neon cooling as a function of: (a) electron density peaking factor, (b) energy enhancement factor f_{H93}, (c) central line averaged electron density, (d) ratio γ of radiated to input power. Asterisks refer to gas puff discharges, while circles and crosses refer to RI mode discharges.

of the radiated power ratio γ, which may significantly change from discharge to discharge for both RI mode and non-RI mode. In Fig. 3 a typical edge electron temperature profile between $r = 44$ cm and $r = 48$ cm is shown for a high density, high γ discharge.

In Fig. 4 the q.n.c. for the RI mode and gas puff discharges of Fig. 2 is displayed as a function of f_p, f_{H93}, $\bar{n}_{e0}$ and γ. Figure 4 includes data points of RI mode discharges (crosses) for which the radial position of the ALT-II limiter was a little displaced with respect to the standard one, resulting in a reduction of the plasma column surface (minor radius $a = 44$ cm) and consequently of q.n.c. of 10%. Moreover, in these discharges the carbon concentration, as measured by CXRS is about 10% higher than in standard discharges. This, however, may cause only a minimal change in the globally measured $P_{rad}/(Z_{eff} - 1)$ both because the cooling efficiency of carbon is not much lower than that of neon for TEXTOR-94 temperatures and because neon is the dominant impurity in these discharges. Therefore, in order to make a correct comparison with the other data of Fig. 4, the 'raw' values of the points marked by crosses have been increased by 15%. This value can, indeed, be taken as an upper limit for the decrease of the q.n.c. related to the displacement of the limiter.

In Figs 4(a) and (b) a reduction of q.n.c. versus f_p and f_{H93} can be seen, while the RI mode data of Fig. 4(c) (circles and crosses) may indicate a tendency for RI mode discharges to display a lower q.n.c. at high density. On the other hand, a relatively high q.n.c. can be achieved also at high electron density ($\bar{n}_{e0}$ comparable with n_{Gr}) if one allows for a strong gas puff (asterisks in Fig. 4(c)). From the data of Fig. 4(d) no significant dependence of q.n.c. on γ can be seen for either RI mode or gas puff mode (Section 3.1).

With respect to the absolute value of q.n.c., comparison with the multimachine Matthews scaling [20] shows that the TEXTOR-94 data which refer to L mode at low $T_e(a)$ are much higher (by a factor of two) than the scaling, while the data of the improved confinement discharges are close to the scaling. For neon the scaling reads: $\{P_{rad}/[Z_{eff}(0) - 1]\}/\bar{n}_{e0}^2 = 0.113S$, where S is the plasma surface in m^2 and $\bar{n}_{e0}$ is expressed in 10^{20} m^{-3}. Since the value of the q.n.c. of the scaling for TEXTOR-94 is 3.6 (10^{-40} MW m^6), one sees that for RI mode discharges q.n.c. can be lower than the scaling, while for gas puff discharges q.n.c. is slightly higher.

The data of the q.n.c. for pure radiofrequency discharges and for RI mode discharges which are shown in Fig. 5 cannot, unfortunately, be quantitatively compared with those of Fig. 4 (gas puff and RI mode). Indeed, in contrast to the data of Fig. 4, the soft X ray spectra of the discharges of Fig. 5 show the presence of iron and chloride lines. Although the correlated plasma contamination did not affect the confinement properties of the discharges, due to a technical problem which lasted only a few days, it did affect Z_{eff}, which was about 20% higher than that for clean discharges. However, in spite of the

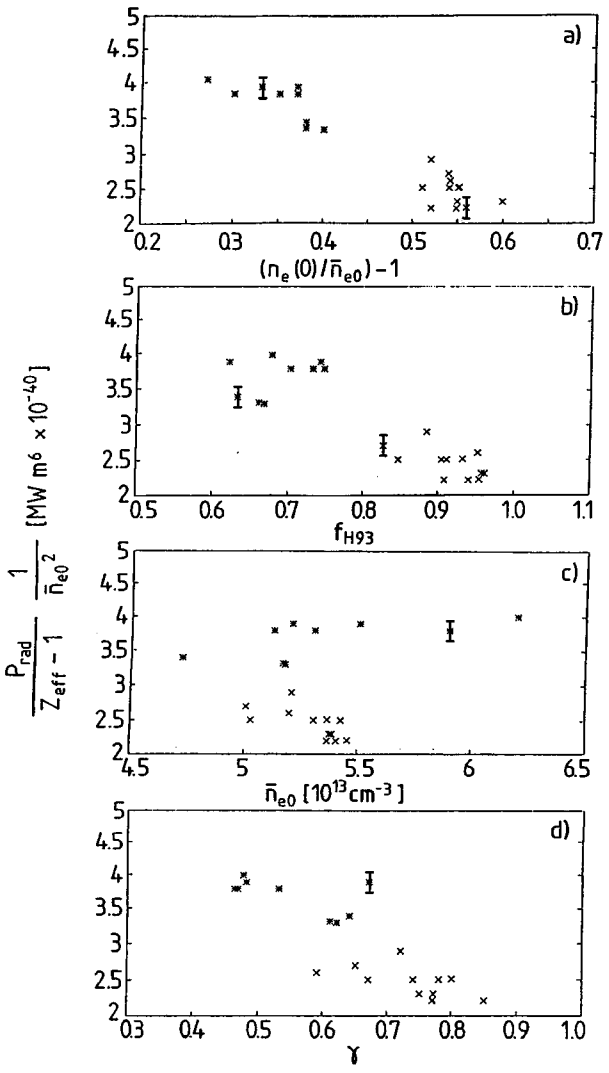

Figure 5. Quality of neon cooling as a function of: (a) electron density peaking factor, (b) energy enhancement factor f_{H93}, (c) central line averaged electron density, (d) ratio γ of radiated to input power. Asterisks refer to pure radiofrequency discharges and crosses refer to RI mode discharges. The discharges in this figure are slightly contaminated by iron and chlorine.

difference in absolute level between the data of Figs 4 and 5, which is quantitatively consistent with the level of high-Z element contamination of the discharges of Fig. 5, the two data sets display a similar dependence of q.n.c. versus the parameters f_p and f_{H93}. The data of Fig. 5 can be seen, therefore, as an extension of the data of Fig. 4 to a slightly different experimental situation.

The asterisks in Fig. 5 label neon seeded discharges at $I_p = 480$ kA either with ICRH only or with ICRH and neutral beam co-injection but P_{NB}/P_{tot} less than 25% (all of these will be referred to as pure radiofrequency discharges) while the RI mode discharges at 400 kA are labelled with crosses. The difference in I_p for the two series implies that the Greenwald density for the pure radiofrequency discharges is higher than that for the RI mode discharges, 7.2×10^{13} and 6.0×10^{13} cm^{-3}, respectively. The reduction of q.n.c. versus f_{H93} and f_p, observed in Fig. 4, is confirmed in the data of Figs 5(a) and (b), and Fig 5(c) confirms that a high q.n.c. can be maintained also at high density, at least up to $\bar{n}_{e0}/n_{Gr} = 0.9$ for the pure radiofrequency discharges. Even though the range of γ for the pure radiofrequency discharges is relatively small, again there is no evidence of a significant γ dependence of q.n.c. within each of the two series of Fig. 5(d).

3.3. The quality of cooling of intrinsic carbon

A first analysis of the quality of carbon cooling (q.c.c.) during neon injection experiments has been done using spectroscopic data and a modified version of the 2-D multifluid code EPIT [21]. The aim of this study is to investigate whether the observed dependence of q.n.c. on f_{H93} and f_p can be confirmed with a similar dependence for the quality of cooling of the residual intrinsic carbon.

The 2-D multifluid code EPIT has been modified, and renamed TECXY [22], to describe the edge plasma of TEXTOR with a toroidal belt limiter. The TECXY code, like most other 2-D computational plasma edge fluid models, is primarily based on the classical transport equations derived by Braginskii. The model describes the electrons and various ion species in their different charge states as separate fluids. The transport along field lines is assumed to be classical and transport coefficients follow from the 21 moment Grad approximation. Radial transport is assumed to be anomalous, with prescribed radial transport coefficients of the order of Bohm diffusion. All ion species have the same temperature T_i, which can be different from the electron temperature T_e. The equations of different fluids are coupled by electrostatic, friction and thermal forces as well as by atomic processes such as collisional ionization, recombination (dielectronic and radiative), excitation and charge exchange. The model allows for arbitrary impurity concentrations, and the non-corona equilibrium distribution of impurity charge states and the corresponding radiated energy losses are determined. The transport of hydrogen (deuterium)

Table 1. Input and output of the TECXY code

Discharge	Input				Output			
	Γ_C (10^{20} s^{-1})	D (m^2 s^{-1})	$n_e(42)$ (10^{13} cm^{-3})	$T_e(42)$ (eV)	$n_e(46)$ (10^{13} cm^{-3})	$T_e(46)$ (eV)	$(P_{rad})_C$ (MW)	$n_C/n_e(42)$ (%)
With gas puff	1.6	0.90	2.80	130	1.00	50	0.253	2.33
RI mode	1.2	0.58	2.55	125	0.83	46	0.128	2.52

and impurity neutrals in the edge of TEXTOR is described by an analytical model which accounts in a self-consistent way for recycling of plasma ions as well as sputtering processes at the limiter surface.

The input data prescribed include the temperature and density of the background plasma at 4 cm inside the LCFS, $T_e(42)$ and $n_e(42)$, the carbon influx from the limiter and the perpendicular diffusion coefficient D. The computed output data include the edge electron density and temperature profiles, the total power radiated by carbon from $r = 50$ cm (4 cm outside the LCFS) up to $r = 42$ cm and the carbon concentration at 4 cm inside the LCFS, $n_C/n_e(42)$. In the few cases examined the reconstructed edge electron temperature and density profiles reproduce well their measured values at the LCFS, $T_e(46)$ and $n_e(46)$.

We report on some details of the results relative to two high performance neon seeded discharges at 400 kA similar in line averaged electron density $\bar{n}_{e0} = 5.9 \times 10^{13}$ cm^{-3} and in normalized beta $\beta_N = 1.45$, but different in f_{H93} and in f_p. For the gas puff discharge (No. 68816) $f_{H93} = 0.83$ and $f_p = 1.37$ while for the RI mode discharge (No. 68825) $f_{H93} = 0.98$ and $f_p = 1.57$. For the gas puff discharge $\gamma = 0.67$ and for the RI mode discharge $\gamma = 0.85$. As one can see in Table 1 the edge electron density is lower in the RI mode discharge (up to 20% depending on radial position) than in the gas puff discharge, while the edge electron temperature profile is very similar for the two discharges.

In order to account for the changes in transport properties of the two discharges we have taken the radial transport coefficients in the code according to the simple estimation $\chi_e = (1/6)a^2/\tau_E$ ($D = \chi_e$, $\chi_i = 0.5\chi_e$), where τ_E is determined by the measured stored energy and input power. This approximation can be justified by the fact that we are interested more in the relative change of the transport coefficients than in their absolute values at the plasma edge. The relevant difference in τ_E in the two discharges (40 and 62 ms, respectively, as compared with only a difference of 20% in f_{H93}) arises from the reduced level of input power needed for the RI mode discharge to reach the same total stored energy of the gas puff discharge. In fact, as mentioned in Section 3.2, the stored energy was kept unchanged in these discharges through a feedback control of the input power level.

Since most of the power radiated by carbon is emitted by the beryllium- and lithium-like carbon ions whose radial position for these discharges is more outwards than 42 cm, $(P_{rad})_c$ computed by TECXY accounts for most of the carbon radiation [14, 23]. As seen in Table 1 the power radiated by carbon in the gas puff case is about twice as high as that in the RI mode case although the ratio of edge carbon concentration to n_e is similar in the two discharges. The C^{6+} concentration in the central plasma for the two discharges as derived from charge exchange recombination spectroscopy (CXRS) is again similar for the two discharges, 0.88 and 0.82% for gas puff and RI mode, respectively, although about a factor of three lower than the total carbon concentration at the edge, computed by TECXY. The n_C/n_e profile seems to be, therefore, largely independent of the electron density peaking factor (Section 4.1). It should be pointed out that in considering typical electron temperature profiles of TEXTOR-94, the CXRS C^{6+} concentration (which is nearly constant along the minor radius in the two discharges) is representative only in the plasma core of the total carbon concentration which at the plasma edge its mostly determined by the lower ionization states. However, the factor of three between computed edge and measured central carbon concentration (which would indicate a strongly hollow concentration

profile) cannot be taken too seriously since the absolute value of the computed n_C/n_e at the edge depends also on the absolute value of the transport coefficients, which have been only roughly estimated.

When the CXRS data for the carbon concentration in the central plasma and the TECXY data for the carbon radiation at the plasma edge are used, the resulting q.c.c. for the gas puff discharge is 2.8×10^{-40} MW m^6 and that for the RI mode discharge is 1.5×10^{-40} MW m^6. These values have to be compared with the measured (globally, with bolometry and bremsstrahlung) q.n.c., which is 4.4×10^{-40} and 3.0×10^{-40} MW m^6 for the two cases, respectively.

The computed reduction of the q.c.c. for the RI mode discharge with respect to the gas puff discharge is, therefore, comparable in relative level with that measured for q.n.c. We can therefore conclude that in TEXTOR-94 plasmas neon and carbon display similar dependences of their radiation properties on transport.

If one assumes the contribution of neon to the total radiated power to be $\Delta P_{rad} = P_{rad} - (P_{rad})_C$, where P_{rad} is measured with bolometry and $(P_{rad})_C$ is the TECXY computed radiation from carbon, and the contribution of neon to the total ionic charge to be $\Delta Z_{eff} = Z_{eff} - (Z_{eff})_C$ where Z_{eff} is measured with bremsstrahlung and $(Z_{eff})_C$ is derived from the CXRS data for the carbon concentration, one can calculate $[\Delta P_{rad}/\Delta Z_{eff}(0)]/\bar{n}_{e0}^2$. The result is $[\Delta P_{rad}/\Delta Z_{eff}(0)]/\bar{n}_{e0}^2$, equal to 4.3×10^{-40} MW m^6 for the gas puff discharge and to 3.2×10^{-40} MW m^6 for the RI mode discharge. These values are very close to those reported above for the measured quantity $\{P_{rad}/[Z_{eff}(0) - 1]\}/\bar{n}_{e0}^2$. This result is expected since in the considered discharges both the edge radiation and the central contamination are dominated by neon (Section 1).

The strong difference in the level of the power radiated by carbon in the two discharges as computed by TECXY is compatible with the observed change in some carbon spectral line intensities. In Fig. 6 the traces of three spectral lines emitted at the plasma edge by C^{2+}, C^{3+} and C^{4+} ions are displayed as a function of the angle of the viewing chords (Fig. 1(b)) for the gas puff and the RI mode discharges. Since the edge electron temperature profile is very similar for the two discharges and the electron density profile is only slightly different, the ratio of the intensity of each of the three spectral lines to the total power emitted by each of the three ions can only marginally change in the two discharges

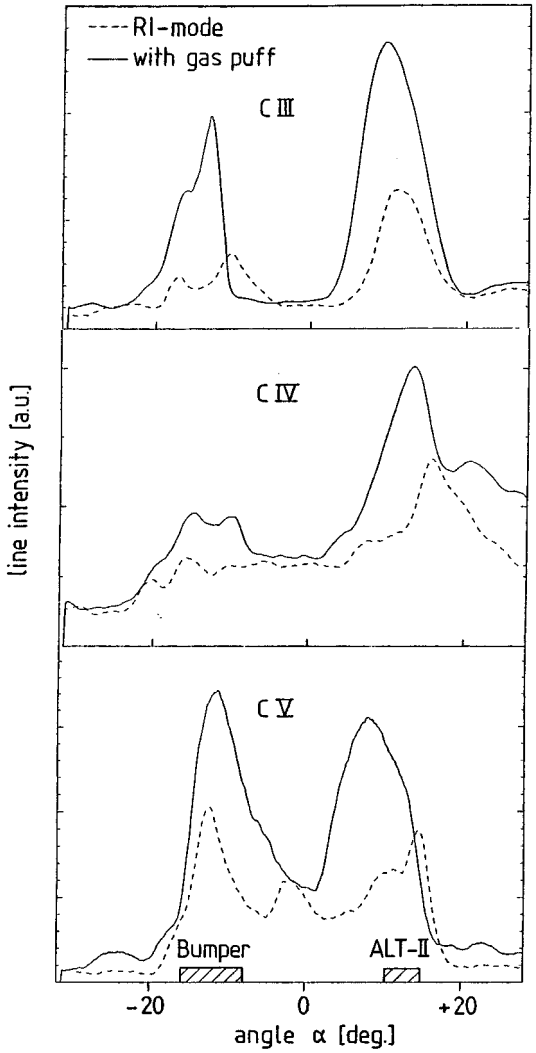

Figure 6. Brilliances of lines emitted by C^{2+}, C^{3+} and C^{4+} ions as a function of the angle α (Fig. 1(b)). The dashed curves refer to an RI mode and the solid curves to a strong gas puff discharge. $\bar{n}_{e0}$ is the same for the two discharges.

[24] (note that the C^{2+} and C^{4+} lines are resonant). Therefore, the computed reduction by TECXY by about a factor of two in the radiated power of carbon for the RI mode discharge as compared with the gas puff discharge is consistent with the observed reduction by about a factor of two in the brilliance of the three carbon spectral lines.

4. Discussion

Although, as pointed out in Section 3.2, the electron temperature profile of the discharges examined in this article may differ at the plasma edge and to

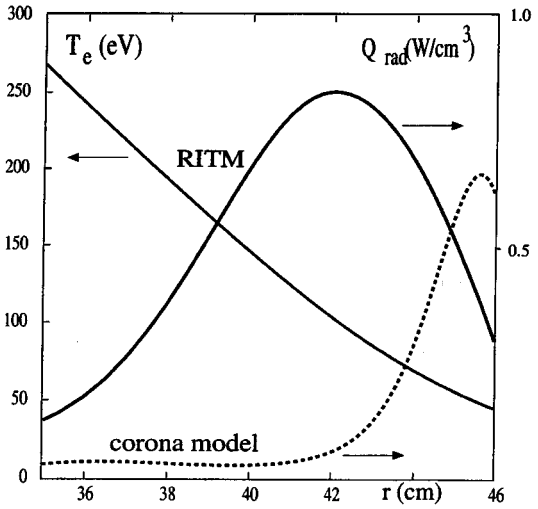

Figure 7. Neon radiated power density, as a function of radius for a typical high density highly radiated power discharge on TEXTOR-94, derived self-consistently from the RITM code. The two curves refer to transport ionization and corona equilibria.

some extent also in the plasma core, this does not affect significantly the q.n.c., as shown by RITM simulations (Figs 7, 10 and Table 2).

Since the edge temperatures of the RI mode discharges are not systematically higher than those of the non-RI mode discharges (in fact they are a little lower on average, see for example Fig. 2), one cannot expect the observed systematic decrease of q.n.c. for the RI mode to be dependent on an edge temperature effect.

In any case a change in edge temperature in the range 50–75 eV cannot cause significant effects on the radiated power level. Indeed, in a transport ionization equilibrium, which is more relevant for tokamak plasmas than for corona plasmas, impurities radiate mainly from the region with a temperature of a half the ionization potential of beryllium- and lithium-like ions, practically independently of discharge conditions. This experimental finding has been confirmed and interpreted on the basis both of simple analytical models and of transport numerical simulations (discussed later). In the case of neon this characteristic temperature slightly exceeds 100 eV. In Fig. 7 the power density of neon radiation is plotted according to transport ionization equilibrium, using the self-consistent RITM code, and to corona equilibrium for a typical high density RI mode TEXTOR-94 discharge. In the case of transport ionization equilibrium not only the integral of Q_{rad} (i.e. P_{rad}) is larger but the Q_{rad} peak value is shifted towards higher temperature regions. This means that a change of the edge temperature from 50 to 75 eV does not lead (in contrast with corona equilibrium predictions) to significant modifications in the total radiation losses: they can change by less than 20%.

Since the quality of neon cooling decreases when both f_{H93} and $f_p = n_e(0)/\bar{n}_{e0}$ increase, the question arises whether this decrease is linked to a change in impurity transport or to a modification of the electron density profile which can affect (also only by geometrical properties) the value of the ratio $P_{rad}/[Z_{eff}(0) - 1]$. $Z_{eff}(0)$, indeed, depends on the central electron density $n_e(0)$ while P_{rad} depends on the edge density, n_e(ed), which decreases slightly with increasing f_p.

The simplest explanation for the reduction of q.n.c. versus f_{H93} and f_p would refer to the possibility that when the electron density profile peaks the impurity density profile peaks more strongly, resulting in the increase of central Z_{eff} for a given edge P_{rad}. Although this possibility is not only hypothetical since it is related to neoclassical impurity inward pinch, both experimental evidence and modelling indicate that an n_i/n_e profile peaking can, at most, be only very marginal:

(a) From the experimental point of view, on the one hand, CXRS data [25] show that the neon density profile peaking is proportional to that of the main ions for a variety of situations which include RI mode discharges. On the other hand, in contrast with situations in which either a high-Z element is involved or sawtooth activity is absent [25, 26], the Z_{eff} profile as derived from bremsstrahlung is flat in the central plasma in all the neon seeded discharges considered here, independently of the value of f_p.

(b) Modelling with the self-consistent RITM code [27] shows that for TEXTOR-94 conditions a neoclassical peaking of the n_i/n_e profile does not occur. The standard model for the particle transport used in RITM calculations includes the particle diffusivity taken as the sum of Alcator scaling, which describes ohmic plasmas, and the Bohm coefficient, which is turned on for auxiliary heated discharges. This model has been validated in simulations of numerous discharges in TEXTOR and TEXTOR-94 by comparison of calculated and measured parameters, for example, the particle confinement time, central density of impurities, integral radiation losses and their volume density, and radiation potential. In the simulations the perpendicular diffusion coefficient of neon

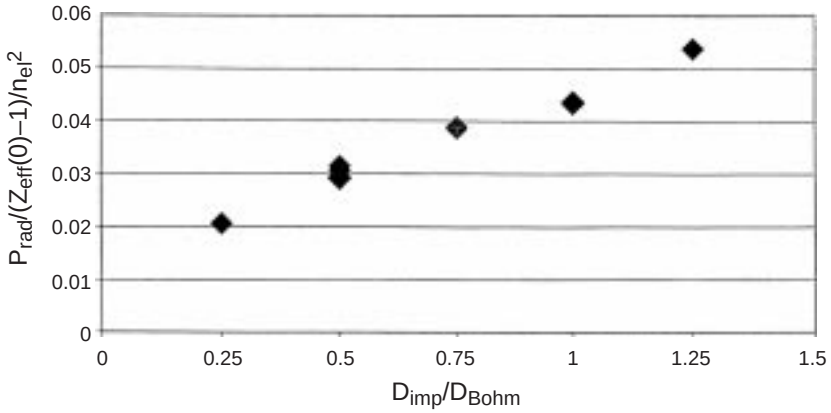

Figure 8. Quality of neon cooling as a function of the neon ion diffusion coefficient. The density shaping factor of background ions S is kept nearly constant at about 2.5. The quality of neon cooling is expressed in units of MW m^6 $\times$ 10^{-38}.

D_{Ne} has been taken as equal to that of the main ions D_D, which is anomalous, Bohm-like. The peaking of the main ion density profile has been varied over a wide range, which covers all the experimental situations in TEXTOR-94, by changing the peaking shaping factor

$$S = \frac{v}{D}\,\frac{a^2}{r}$$

from 1.5 to 3.5 (D and v are the diffusivity and the inward velocity of the main ions). For each value of S (of the main ions) the neoclassical pinch velocity of the neon ions has been computed as well as the corresponding neon ion density profiles (Z_{eff}) and the neon-line radiation (P_{rad}).

The resulting RITM computed q.n.c. does not show any dependence on the value of S but remains practically constant at about 4 [10^{-40} MW m^6]. This result can be understood by considering that for the relevant TEXTOR-94 conditions the highly ionized neon ions are in the plateau collisionality regime (where an inward pinch can prevail [27]) only in the inner half of the minor radius, while in the outer half they are in the Pfirsch–Schlüter regime. Here the inward drift caused by the density gradient of the background ions is balanced by an outward drift due to the gradient of the background ion temperature (temperature screening).

Excluding then for TEXTOR-94 discharges a correlation between f_p and n_i/n_e profile peaking, two other phenomena can lead to the observed reduction of q.n.c. with increasing confinement.

(1) Finite impurity residence time. It is well known [23, 28, 29] that, for given impurity and electron edge densities, different levels of power can be radiated, even for unchanged temperature, depending on the impurity confinement time (more specifically on the impurity diffusivity). Indeed, since the volume V_L of the plasma where line radiation is emitted depends also on impurity transport and increases when transport increases, P_{rad}, which is given by $n_i n_e L_i(T_e) V_L$, can change even at $n_i n_e L_i(T_e)$ constant. RITM simulations confirm such a dependence of the power radiated level on impurity transport. Runs have been made in which both the parameters S and D_D (of the main ions) are maintained nearly constant ($D_D = D_{Bohm}$) while the impurity diffusion coefficient D_{imp} is scanned over a wide range, Fig. 8. In fact, unlike the above reported RITM simulations, in these runs D_{imp} has not been set equal to D_D. For each value of D_{imp} the impurity drifts have been computed according to neoclassical theory, as well as the related P_{rad} and Z_{eff}, as in the previously reported simulations. The computed q.n.c. are plotted as a function of D_{imp}/D_{Bohm} in Fig. 8, where one sees that, in contrast with the RITM results concerning the scan of the shaping parameter S for the main ions, a change in D_{imp} causes a significant change in q.n.c.

(2) A second mechanism which can lead to a reduction of q.n.c. with increasing confinement is a change of edge electron density n_e(ed). Since, at a given $\bar{n}_{e0}$, n_e(ed) decreases slightly with increasing f_p, P_{rad}, which is proportional to the product

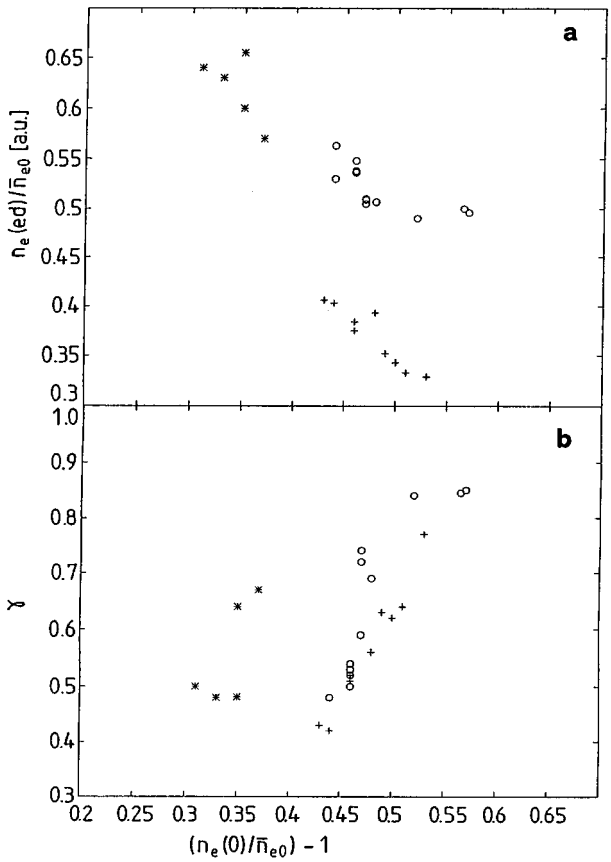

Figure 9. (a) Ratio between line integrated edge and central electron densities as a function of the density peaking factor. In the series marked by asterisks and circles, the edge density is measured 2 cm more inwards than in the series marked with crosses. (b) Radiated power ratio γ as a function of the density peaking factor for the discharges of Fig. 9(a).

$n_i n_e$(ed), can also decrease for a given edge impurity density.

The TEXTOR-94 data indicate that both mechanisms (1) and (2) contribute to the observed level of decrease of q.n.c. versus f_p. In fact, the reduction of n_e(ed) can be responsible only for a part of the total reduction of q.n.c. with increasing f_p. In Fig. 9(a) the ratio between n_e(ed) and $\bar{n}_{e0}$ is shown as a function of f_p for the series of discharges of Fig. 4. For the series labelled with asterisks and circles, n_e(ed) is the line averaged density at about $r = 40$ cm, n_{e40} (i.e. 6 cm inside the LCFS), while for the series labelled with crosses n_e(ed) is the line averaged density at about $r = 42$ cm, n_{e42} (i.e. 4 cm inside the LCFS). In both cases the reduction of n_e(ed) with increasing f_p is about 25% as compared with a reduction of about 50% in the q.n.c. at high f_p.

The relatively rapid decrease of n_e(ed)/$\bar{n}_{e0}$ with increasing f_p as appears in Fig. 9(a) arises from the superposition of two different mechanisms:

(a) The simple geometrical fact that increasing f_p causes a slight reduction of the edge density,
(b) The experimental fact that some data points at higher f_p considered in the present analysis are, by chance, also at higher γ, see Fig. 9(b). (High f_p and f_{H93} can also be obtained at moderate γ, see Section 3.1).

Therefore, since an increase of γ causes a decrease of edge electron density and, even more strongly, of temperature [18], the global effect on q.n.c. is expected to be modest since the higher value of the cooling rate $L(T_e)$ tends to compensate for the decrease of n_e(ed).

Finally, we want to discuss the influence of the electron temperature profiles on q.n.c. and to discriminate this influence from the effect of the impurity diffusion coefficient as described above. For this purpose we performed, with the RITM code, self-consistent calculations of energy and particle transport (background and impurity ions) for two TEXTOR-94 discharges, which are comparable to those already shown in Fig. 4 and referred to as 'RI mode' and 'gas puff' discharges. In these calculations the shaping factor for the density profile of the background ions has been adapted to match the experimental density profile as the heat diffusivities of electrons and ions (governing the conductive energy transport in the core and assumed to be gyro-Bohm-like [27]) were scaled to match the energy confinement. No attempt was made to include a more proper description of the heat transport taking into account the effect of ITG mode stabilization (as the physical mechanism governing the transition to RI mode as discussed in Ref. [30]), since the dominating influence of the impurity diffusivity on q.n.c. will mainly be illustrated.

Both discharges (No. 68803 (RI mode) and No. 68817 (gas puff)) are heated by $P_{tot} = 2.6$ MW with a fraction of radiated power $P_{rad}/P_{tot} = 70\%$. The first discharge has an energy confinement time with respect to ELM-free H mode scaling of $f_{H93} = \tau_{-E}/\tau_{-ITER93\text{-}H} = 1.0$, and the second discharge has one of $f_{H93} = 0.8$. Within the calculations, the particle diffusivities of both the main and impurity ions at the edge have been assumed to be half the Bohm value for the high confinement discharge

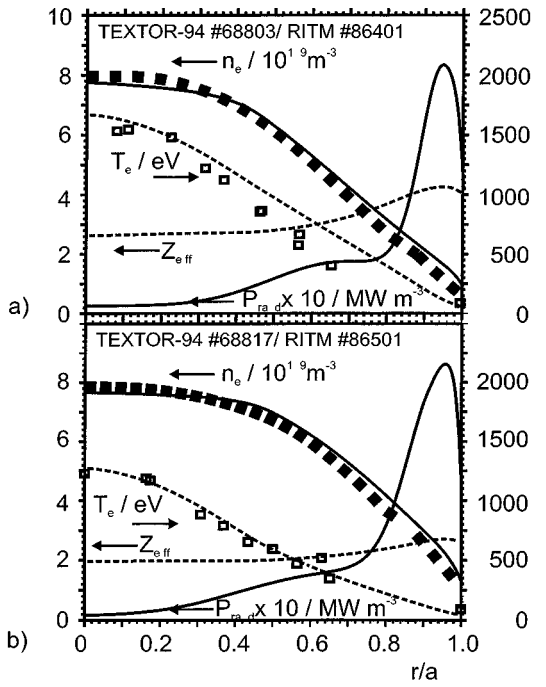

Figure 10. Radial profiles of electron density, electron temperature, Z_{eff} and radiated power density (solid and broken curves) as calculated with the RITM code for TEXTOR-94 discharges (a) No. 68803 and (b) No. 68817. Experimental data for electron temperature (open boxes) and electron density (filled boxes) are shown for comparison.

68803 and equal to the Bohm value for the gas puff discharge 68817. Neon is added in the calculations to match the experimental fraction of radiated power. It should be pointed out that the levels of electron temperature for discharges 68803 and 68817 represent, respectively, the upper and lower limits for the temperatures of all the discharges examined in this article.

The results of the modelling are shown in Fig. 10(a) for discharge 68803 and in Fig. 10(b) for discharge 68817. The solid and dashed lines show the modelled radial profiles of the electron density and temperature, the radiated power density and Z_{eff}. For comparison the experimental electron temperature profile (measured with an ECE diagnostic in the core and a thermal helium beam diagnostic at the edge, open boxes) and electron density profile (measured with the HCN interferometer, filled boxes) are included. Both cases show reasonable agreement between experiment and self-consistent transport modelling. For further discussion a third calculation was made to combine the lower heat transport (higher energy confinement) with the higher impurity transport $D = D_{Bohm}$, a combination not seen in the experiments. Table 2 summarizes the relevant findings with respect to the relation between heat and particle transport and the resulting q.n.c. The increase of the edge diffusivity in the calculation for discharge 68817 leads to an increase of the q.n.c. from 3.7×10^{-40} MW m^6, found in the calculation for discharge 68803, to 6.2×10^{-40} MW m^6. This change clearly confirms the experimental findings shown in Fig. 4. It should be stressed that the computed reduction of q.n.c. for discharge 68803 with respect to that for discharge 68817 is not linked to the increase of electron temperature of the discharge at improved energy confinement, as proven by the third calculation, where a q.n.c. as high as 5.6×10^{-40} MW m^6 is found, with a temperature profile comparable to that of discharge 68803. The same conclusions can be drawn from calculations of q.n.c. with the help of a trace (collisional–radiative) impurity transport code [31], using experimental profiles as input data. It is found that the impurity diffusion coefficient is the most relevant parameter in determining the cooling efficiency, in accordance to the self-consistent calculations described above.

A simple analytical expression for the ratio $P_{rad}/[Z_{eff}(0) - 1]$ can be helpful in summarizing the main points discussed above. For an impurity which radiates only at the plasma edge, one has from Ref. [29]:

$$\frac{P_{rad}}{Z_{eff}(0) - 1} \propto \frac{n_{imp}(\mathrm{ed})}{n_{imp}(0)}\, n_e(0) \sqrt{n_e(\mathrm{ed})}\, \sqrt{D_{imp}(\mathrm{ed})}. \tag{1}$$

In fact

$$Z_{eff}(0) - 1 \propto \frac{n_{imp}(0)}{n_e(0)}$$

and $P_{rad} \propto n_e(\mathrm{ed}) n_{imp}(\mathrm{ed}) \Delta r$, where Δr is the thickness of the radiative layer and

$$\Delta r = \sqrt{D_{imp}(\mathrm{ed}) \tau_{ion}^{imp}} \propto \sqrt{\frac{D_{imp}(\mathrm{ed})}{n_e(\mathrm{ed})}} \tag{2}$$

where τ_{ion}^{imp} is the impurity ionization time.

The experimental results of TEXTOR-94 and the RITM simulations can, therefore, be interpreted as follows: for the prevailing TEXTOR-94 conditions, at given $\bar{n}_{e0}$ and γ, a change in the electron density profile is accompanied by a change in the impurity density profile such that the variations in

$$\frac{n_{imp}(\mathrm{ed})}{n_{imp}(\mathrm{ed})}\, n_e(\mathrm{ed}) \sqrt{n_e(\mathrm{ed})}$$

Table 2. Results from modelling with the self-consistent RITM code

TEXTOR-94 discharge	$D_{i,main+imp}$ RITM input	P_{rad}/P_{tot} calculated (%)	$\{P_{rad}/[Z_{eff}(0)-1]\}/\bar{n}_{e0}^2$ (10^{-40} MW m^{-6}) calculated	$T_e(0)$ (eV) calculated
68803	$0.5 \times D_{Bohm}$	70	3.7	1664
68817	$1 \times D_{Bohm}$	70	6.2	1258
	$1 \times D_{Bohm}$	70	5.6	1605

are of minor importance. On the other hand, the increase of D_{imp} causes an increase in the quality of impurity cooling (the exact functional dependence is not a crucial point at this stage). Although according to Eq. (1) the q.n.c. should scale as $(n_e)^{-0.5}$ such a density dependence of the q.n.c. is not experimentally observed (see, for example, Fig. 5(c) for radiofrequency discharges and Ref. [11]). It should be pointed out that the edge temperature dependence of $L(T_e)$, and consequently of the quality of impurity cooling, has not been considered in Eq. (1).

We have established from simulations and general arguments (see, e.g., Table 2 and Fig. 7) that the observed differences in neon cooling efficiency among the discharges examined can be only marginally dependent on a temperature effect. Moreover, for the TEXTOR-94 neon collisionality regimes a peaking of the n_{Ne}/n_e profile (which would account for the reduction of q.n.c. at high f_p) has not been observed experimentally and is not predicted to occur. On the other hand, RITM simulations predict, in agreement with a simple analytical shell model (Eq. (2)), that total radiated power increases with impurity particle diffusivity. This result, which is independent of the transport model used, can be explained by the following argument. Radiating impurity species are ionized in the region where an electron temperature of a half of their ionization potential is reached. The only dependence of their lifetime on plasma parameters is an inverse proportionality to electron density. Thus, the distance travelled by radiating particles during their life is proportional to the square root of the ratio of the diffusivity to the electron density. This distance gives roughly the width of the radiating layer.

5. Conclusions

Both the TEXTOR-94 high density radiative regimes considered, RI mode and pure radiofrequency/gas puff mode, display good confinement properties, the capability of achieving electron densities of the order of the Greenwald density and radiative power exhaust at Z_{eff} between 2 and 3, depending on the level of electron density and of P_{rad}. While for the pure radiofrequency/gas puff mode both confinement and impurity radiation efficiency are relatively constant with respect to a change in $\bar{n}_{e0}$, for RI mode the confinement increases and the impurity radiation efficiency decreases with increasing $\bar{n}_{e0}/n_{Gr}$. Consequently, at high values of $\bar{n}_{e0}/n_{Gr}$ (of the order of or above one) not only the confinement enhancement factor f_{H93} of RI mode can be significantly higher than that of the pure radiofrequency/gas puff mode but also Z_{eff} in the plasma core can be higher for RI mode, for a given level of power radiated at the plasma edge.

For scenarios with a radiative mantle the increase of Z_{eff} with increasing confinement is not an aspect peculiar to TEXTOR-94 discharges. Indeed, from self-consistent simulations based on standard transport models, impurity particle diffusivity at the edge appears to be the decisive parameter in determining the level of the radiated power for a given impurity species and a given level of the main plasma contamination.

Acknowledgements

The authors would like to thank M.E. Puiatti for providing us with the results of the simulations performed with the impurity transport code described in Ref. [31].

References

[1] Samm, U., et al., Plasma Phys. Control. Fusion **34** (1993) B167.
[2] Telesca, G., et al., Nucl. Fusion **36** (1996) 347.
[3] Messiaen, A.M., et al., Phys. Plasmas **4** (1997) 1690.
[4] Ongena, J., et al., in Controlled Fusion and Plasma Physics (Proc. 24th Eur. Conf. Berchtesgaden, 1997), Vol. 21A, Part IV, European Physical Society, Geneva (1997) 1693.

[5] Keilhacker, M., JET Team, Plasma Phys. Control. Fusion **37** (1995) A3.
[6] Neuhauser, J., et al., Plasma Phys. Control. Fusion **37** (1995) A37.
[7] Telesca, G., et al., in Controlled Fusion and Plasma Physics (Proc. 24th Eur. Conf. Berchtesgaden, 1997), Vol. 21A, Part IV, European Physical Society, Geneva (1997) 1725.
[8] Kallenbach, A., et al., ibid., p. 1473.
[9] Gruber, O., et al., Plasma Phys. Control. Fusion **39** (1997) B19.
[10] Wade, M.R., et al., J. Nucl. Mater. **266–269** (1999) 44.
[11] Telesca, G., et al., J. Nucl. Mater. **241–243** (1997) 853.
[12] Foord, M.E., et al., Rev. Sci. Instrum. **53** (1982) 1407.
[13] Telesca, G., et al., in 1992 International Conference on Plasma Physics (Proc. Conf. Innsbruck, 1992), Vol. 16C, Part II, European Physical Society, Geneva (1992) 1147.
[14] Telesca, G., et al., Nucl. Fusion **34** (1994) 625.
[15] Pospieszczyk, A., et al., J. Nucl. Mater. **162–164** (1989) 574.
[16] Schweer, B., et al., J. Nucl. Mater. **198–198** (1992) 174.
[17] Rapp, J., Ortsaufgeloeste Messung der Strahlungsleistung des TEXTOR-Plasmas in einem poloidalen Querschnitt, Rep. Jul-3172, Forschungszentrum Jülich (1996).
[18] Unterberg, B., et al., Plasma Phys. Control. Fusion **39** (1997) B189.
[19] Hobirk, J., et al., in Controlled Fusion and Plasma Physics (Proc. 24th Eur. Conf. Berchtesgaden, 1997), Vol. 21A, Part IV, European Physical Society, Geneva (1997) 1861.
[20] Matthews, G.F., et al., J. Nucl. Mater. **241–243** (1997) 450.
[21] Zagorski, R., J. Tech. Phys. **37** (1996) 7.
[22] Zagorski, R., et al., Contrib. Plasma Phys. **38** (1998) 61.
[23] Samm, U., Transactions of Fusion Technology, Vol. 25, No. 2T, Part 2 (1994) 259.
[24] Kubo, H., et al., Plasma Phys. Control. Fusion **37** (1995) 1133.
[25] Jaspers, R., et al., in Controlled Fusion and Plasma Physics (Proc. 24th Eur. Conf. Berchtesgaden, 1997), Vol. 21A, Part IV, European Physical Society, Geneva (1997) 1713.
[26] Rapp J., et al., Plasma Phys. Control. Fusion **39** (1997) 1615.
[27] Tokar', M.Z., Plasma Phys. Control. Fusion **36** (1994)
[28] Carolan, P.G., Piotrowicz, V.A., Plasma Phys. Control. Fusion **25** (1983) 1065.
[29] Tokar', M.Z., Nucl. Fusion **34** (1994) 853.
[30] Tokar', M.Z., et al., Plasma Phys. Control. Fusion **41** (1999) B317.
[31] Mattioli, M., et al., Phys. Rev. E **60** (1999) 4760.

(Manuscript received 12 February 1999
Final manuscript accepted 2 August 2000)

E-mail address of G. Telesca:
Telesca@igi.pd.cnr.it

Subject classification: F1, Te; I1, Te; J1, Te